Motion and rigidity of the Pacific Plate and implications for plate boundary deformation

J. Beavan,[1] P. Tregoning,[2] M. Bevis,[3] T. Kato,[4] and C. Meertens[5]

Received 11 August 2000; revised 8 January 2002; accepted 13 January 2002; published 26 October 2002.

[1] Using up to 11 years of data from a global network of Global Positioning System (GPS) stations, including 12 stations well distributed across the Pacific Plate, we derive present-day Euler vectors for the Pacific Plate more precisely than has previously been possible from space geodetic data. After rejecting on statistical grounds the velocity of one station on each of the Pacific and North American plates, we find that the quality of fit of the horizontal velocities of 11 Pacific Plate (PA) stations to the best fitting PA Euler vector is similar to the fit of 11 Australian Plate (AU) velocities to the AU Euler vector and ~20% better than the fit of nine North American Plate (NA) velocities to the NA Euler vector. The velocities of stations on the Pacific and Australian Plates each fit a rigid plate model with an RMS residual of 0.4 mm/yr, while the North American velocities fit a rigid plate model with an RMS velocity of 0.6 mm/yr. Our best fitting PA/AU relative Euler vector is located ~170 km southeast of the NUVEL-1A pole but is not significantly different at the 95% confidence level. It is also close (<70 km in position and <3% in rate) to a pole derived from transform faults identified from satellite altimetry, suggesting that the vector has not changed significantly over the past 3 Myr. Our relative Euler vector is also consistent with all known geological and geodetic evidence concerning the AU/PA plate boundary through New Zealand. The GPS sites offshore of southern California are presently moving 4–5 ± 1 mm/yr relative to predicted Pacific velocity, with their residual velocities in approximately the opposite direction to PA/NA relative motion. Likewise, the easternmost sites in South Island, New Zealand, are moving ~3 ± 1 mm/yr relative to predicted Pacific velocity, with the residuals in approximately the opposite direction to PA/AU relative motion. These velocity residuals are in the same sense as predicted by elastic strain accumulation on known plate boundary faults but are of a significantly higher magnitude in both southern California and New Zealand, implying that the plate boundary zones in both regions are wider than previously believed. *INDEX TERMS:* 1206 Geodesy and Gravity: Crustal movements—interplate (8155); 1208 Geodesy and Gravity: Crustal movements—intraplate (8110); 1243 Geodesy and Gravity: Space geodetic surveys; 8158 Tectonophysics: Evolution of the Earth: Plate motions—present and recent (3040); 8159 Tectonophysics: Evolution of the Earth: Rheology—crust and lithosphere; *KEYWORDS:* Pacific plate motion, plate rigidity, plate boundary deformation

Citation: Beavan, J., P. Tregoning, M. Bevis, T. Kato, and C. Meertens, Motion and rigidity of the Pacific Plate and implications for plate boundary deformation, *J. Geophys. Res.*, *107*(B10), 2261, doi:10.1029/2001JB000282, 2002.

1. Introduction

[2] A number of studies over the past 6 years have estimated present-day relative motions of the major tectonic plates by inverting geodetic station velocities determined from space-geodetic data at sites distributed across the plates, thereby determining the Euler vectors describing the relative rotation between the plates. These motions have been compared with 3-Myr average motions deduced from seafloor spreading and earthquake slip direction data, in particular the NUVEL-1A model of *DeMets et al.* [1994], in order to test the stability of plate motions through time.

[3] Relative Euler vectors so derived make predictions about the relative motions along any part of the common boundary between a pair of plates. In places where detailed measurements can be made across the plate boundary, such measurements can test the predictions of the plate model and can lead to insights about the plate boundary kinematics and dynamics.

[1]Institute of Geological and Nuclear Sciences, Lower Hutt, New Zealand.
[2]Research School of Earth Sciences, Australian National University, Canberra, Australia.
[3]School of Ocean and Earth Science and Technology, University of Hawaii, Honolulu, Hawaii, USA.
[4]Earthquake Research Institute, University of Tokyo, Tokyo, Japan.
[5]University NAVSTAR Consortium, Boulder, Colorado, USA.

0148-0227/02/2001JB000282$09.00

[4] If station velocities are available at points well distributed through the interior of a plate it is possible to test the rigidity of the plate by examining how well the velocities can be fit by a single Euler vector relative to some conventional reference frame such as the ITRF97 realization of the International Terrestrial Reference Frame [*Boucher et al.*, 1999]. The sizes of the misfits can give a measure of the internal rigidity of the plate, thereby testing a fundamental assumption of plate tectonics. A number of recent studies have done this for the North American, Eurasian and Australian Plates [e.g., *Dixon et al.*, 1996; *DeMets and Dixon*, 1999; *Kogan et al.*, 2000; *Tregoning*, 2002b].

[5] Until recently, the motion of the largest plate, the Pacific Plate, has been poorly determined because there have been only a few space-geodetic sites on the plate. This has affected the accuracy of the relative Euler vectors between the Pacific Plate and its neighbors. As recently as 1997, *Larson et al.* [1997] had available only three Pacific Plate sites, one of which had a very short data series while a second had particularly noisy data. *Tregoning et al.* [1998] used two sites in the Pacific interior plus an additional four near the Pacific/North Bismarck plate boundary, which they believed were moving with Pacific Plate velocity based on the data available at the time. *DeMets and Dixon* [1999] and *Tregoning* [2002b] have used five and six sites, respectively, in the Pacific interior. There has been a wide scatter in the estimates of pole position and rate between the Pacific Plate (PA) and the North American (NA) and Australian (AU) Plates (see, for example, Table 3 later in this paper).

[6] The various Euler vector estimates make predictions which are sufficiently different that they can be compared with each other and tested against ground observations. For example, the rate of shortening normal to the plate boundary across the South Island of New Zealand varies by more than a factor of 2 between different models. *Larson et al.*'s [1997] PA/AU Euler vector derived from Global Positioning System (GPS) data predicts 16.1 ± 3.0 mm/yr shortening at latitude 43.5°S while all more recently published GPS-based estimates predict shortening rates close to or lower than the NUVEL-1A value of 9.5 ± 2.0 mm/yr.

[7] The difference between the NUVEL-1A 3-Myr average and some of the present-day estimates has led to speculation that the PA/AU and PA/NA Euler vectors have changed with time over the past 3 Myr. Such speculation is enhanced by the well-documented changes in pole position that have occurred for PA/AU between 17.5 Ma and 6.4 Ma (reviewed by *Walcott* [1998]) and for PA/NA at approximately 8 Ma [*Atwater and Stock*, 1998]. *DeMets and Dixon* [1999] give the most recent discussion of changes in PA/NA motion, and conclude both that the rate has been steady over the past 3 Myr and that the NUVEL-1A model underestimates PA/NA motion in the western United States by 4 ± 2 mm/yr.

[8] In this paper we have combined GPS data collected by New Zealand, Japanese, and U.S. organizations over the past 11 years with publicly available International GPS Service (IGS) data to determine horizontal velocities of 12 stations at 11 sites well distributed across the Pacific Plate (Figure 1a). This allows us to calculate the PA/AU and PA/NA Euler vectors more precisely than has previously been possible and to test for internal deformation within the Pacific Plate. In regard to internal deformation we note that analyses by *DeMets and Dixon* [1999] and *Tregoning* [2002b] have found small and perhaps significant velocity residuals at station CHAT relative to their best fitting PA Euler vectors, while *Kogan et al.* [2000] found a significant velocity residual at station FAIR relative to their best fitting NA Euler vector. We also analyze the horizontal velocities of stations along the western coast and offshore islands of California and along the east coast of South Island, New Zealand, in order to determine whether these stations are moving with Pacific Plate velocity and, if not, what implications there may be for offshore deformation at these plate boundaries.

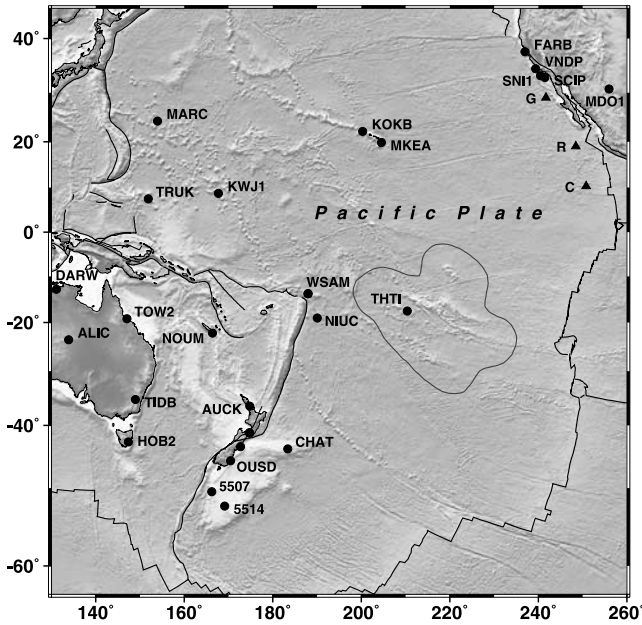

Figure 1a. GPS stations (dots) in and around the Pacific with shaded relief bathymetry lit from the north-northwest. The grey contour in the central South Pacific shows the approximate outline of a model of the South Pacific Superswell proposed by *McNutt and Fischer* [1987] but whose existence has been questioned by *Levitt and Sandwell* [1996]. The triangles denote islands in the eastern Pacific which, if instrumented with GPS receivers, would provide additional control on Pacific plate motion and deformation offshore of California (G, Isla de Guadalupe; R, Islas Revillagigedos; C, Clipperton Island). Details near California and New Zealand are given in Figures 1b and 1c.

2. Tectonic Setting

[9] The Pacific Plate is the largest of the Earth's tectonic plates and is predominantly oceanic. Because of their olivine-rich chemistry, oceanic plates are thought to be significantly more rigid than their continental counterparts. It is certainly true that plate boundary deformation zones in continental crust are generally far wider (tens to hundreds of kilometers) than the narrow (<10 km) boundaries typically found in oceanic plates.

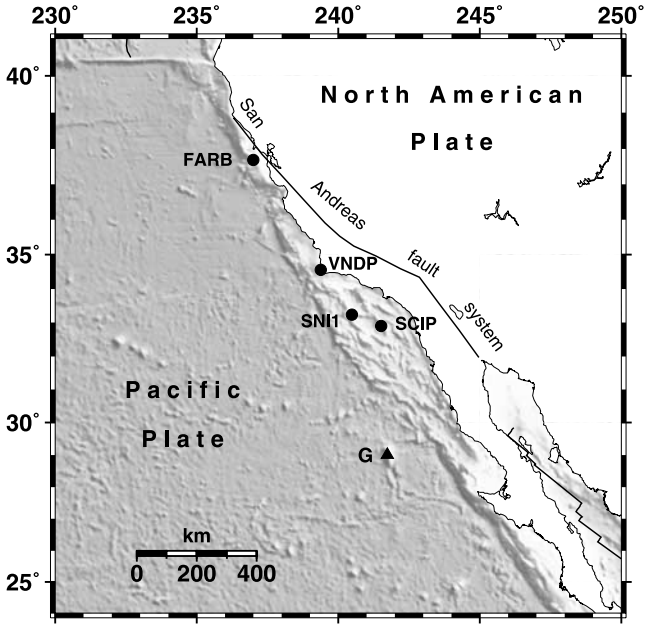

Figure 1b. GPS stations and tectonic features of interest offshore of California, with shaded relief bathymetry lit from the northeast. Note the substantial structure in the continental shelf offshore of VNDP and the Channel Island stations, SCIP and SNI1. The scale bar shows true scale at latitude 32°N.

[10] Land occurs on both sides of the boundary of the Pacific Plate and its neighboring plates in only three regions: (1) California and northern Mexico, (2) western Canada and southeast Alaska, and (3) the South Island of New Zealand. In all cases, the boundary is on land because of the presence of a small amount of continental crust near the edge of the Pacific Plate. New Zealand and California are the more accessible regions for making measurements, and extensive geodetic observations have been made in both regions, especially over the last 10–15 years. Constraining interplate motion using land-based measurements across the plate boundary in California (and especially northern and central California) is complicated because of the extreme width of the boundary zone (including the Basin and Range province) between the stable interiors of the PA and NA plates. By contrast, in New Zealand the entire interplate deformation is believed to occur within <300 km.

[11] In California (Figure 1b) the interplate motion is generally 40–50 mm/yr right-lateral strike slip along the San Andreas system (where the system encompasses the network of sub-parallel faults that are present along most of the boundary [e.g., *Feigl et al.*, 1993; *Bennett et al.*, 1996; *Freymueller et al.*, 1999; *Savage et al.*, 1999]). An extensional component to the PA/NA motion at the latitudes of northern and central California is accommodated by east-west extension in the Basin and Range. In southern California there are known active faults offshore as far southwest as the San Clemente Fault (which runs 10 km northeast of station SCIP), but the substantial structure in the continental shelf bathymetry (Figure 1b) suggests that there could be additional active deformation farther offshore.

[12] North of New Zealand (Figure 1c), Pacific Ocean floor is being subducted at the Tonga-Kermadec Trench. Toward the southern end of this trench, where it is named the Hikurangi Trough, there is a triangular region of atypical seafloor being subducted. This, the Hikurangi Plateau, is an oceanic plateau at 2500–3500 m depth consisting of either thickened oceanic or thinned continental crust. Farther south, subduction dies out and becomes oblique continental collision because of the presence of continental crust on both sides of the plate boundary: the Chatham Rise and Campbell Plateau on the Pacific side and the Challenger Plateau on the Australian side.

[13] In the South Island of New Zealand the relative plate motion is 35–40 mm/yr right lateral along the Alpine fault system but with a substantial convergent component of ~10 mm/yr. *Walcott* [1998] reviews the modes of oblique convergence in the South Island. Broadly speaking, deformation north of about Christchurch (station 5508) is largely taken up by a system of strike-slip faults sub-parallel to the relative plate motion direction. South of this strike-slip system the main plate boundary fault (the Alpine Fault) is oriented more northerly and the contractional component of motion is taken up by continental collision that has been building the Southern Alps for at least the past 6.4 Myr. Farther south, the continental collision zone broadens con-

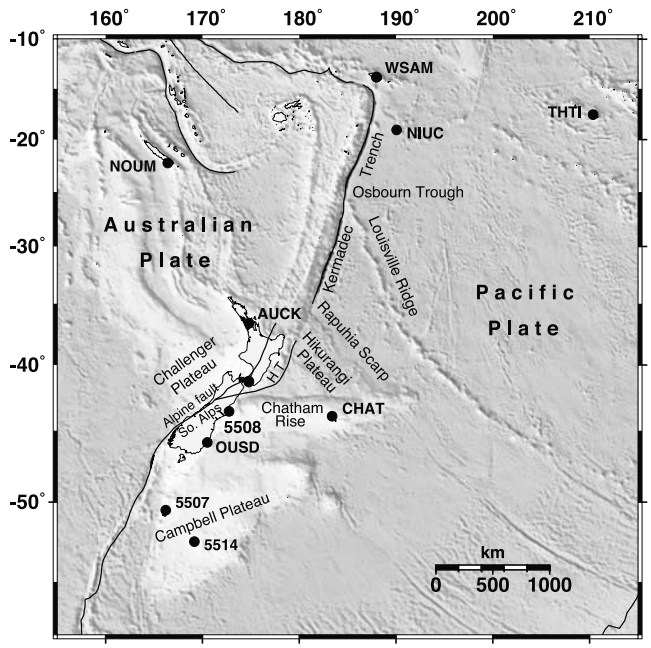

Figure 1c. GPS stations and major tectonic features of interest in the New Zealand region, with shaded relief bathymetry lit from the southwest. "HT" denotes the Hikurangi Trough, the southern end of the Tonga-Kermadec Trench. The triangular Hikurangi Plateau is an oceanic plateau being subducted at the Hikurangi Trough. It consists of a region of thickened ocean crust or thinned continental crust with the Rapuhia Scarp and Chatham Rise forming its northeastern and southern boundaries. The Chatham Rise and Campbell Plateau are an area of continental crust on the Pacific Plate that is colliding obliquely with the Challenger Plateau continental crust on the Australian Plate. The scale bar shows true scale at latitude 40°S.

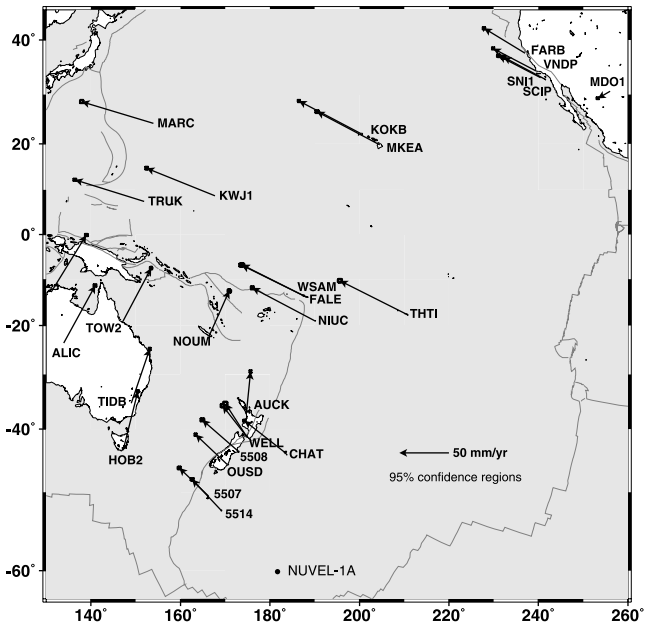

Figure 2. GPS velocities at Pacific Plate and adjacent stations in the ITRF2000 reference frame with 95% confidence uncertainty ellipses. The velocity vectors are shown for both the WELL and WGTN sites in Wellington, New Zealand, but for clarity only WELL is labeled. The position of the NUVEL-1A AU/PA relative pole is shown for reference.

siderably, with the deformation front occurring some 20 km offshore to the east in the vicinity of Dunedin (station OUSD) [e.g., *Litchfield and Norris*, 2000].

3. Geodetic Data

[14] The geodetic data used in this analysis have been sourced from global tracking stations of the IGS, from campaign-style GPS surveys in the western and southwest Pacific and from several continuously operating stations that form part of the WING network [*Kato et al.*, 1998], the University of Hawaii SW Pacific network [*Bevis et al.*, 1995; *Taylor et al.*, 1995], and the New Zealand continuous GPS network.

[15] The Pacific Plate GPS sites (Figures 1 and 2) span the plate from its eastern edge at the California coast to western boundary sites in New Zealand, Samoa, Micronesia and the North Pacific. The only land areas not well sampled are in the central South Pacific, such as Kiribati, the Line Islands, and much of French Polynesia. Other potential plate interior sites for which we have no data are several islands well offshore of Mexico: Guadalupe Island, the Revillagigedo Islands and Clipperton Island (though the latter site may not be on the rigid Pacific Plate because of its location in the Clipperton fracture zone).

[16] Table 1 gives information about the site occupations and lengths of time series used in this analysis. We concentrated on analyzing long spans of data rather than a large number of days of data, since experience has shown that long data series are the best way to achieve stable and reliable velocity solutions (assuming the velocity is constant over the duration of the measurements). This experience is supported by the noise model results discussed below. To this end, we extended the continuous data series at station TRUK (Figures 1a and 2) by incorporating 1994 and earlier data from campaign station XAVR using a site tie measured in 1996 ($\Delta H = -1.5904$ m, $\Delta E = 0.3291$ m, $\Delta N = 1.8970$ m from TRUK to XAVR in the ITRF97 reference frame). We note that data following the M_W 7.8 Indian Ocean earthquake of 18 June 2000 were not used to estimate the velocity of station COCO, since the earthquake caused an estimated offset of ~35 mm at this station [*Tregoning*, 2002a].

3.1. Data Analysis

[17] The data were analyzed as daily global solutions using the GAMIT/GLOBK software [*King and Bock*, 1999; *Herring*, 1999] to combine regional data with data from up to 80 IGS stations. We solved for a free-network global polyhedron which we then aligned with the ITRF2000 reference frame [*Altamimi et al.*, 2002] by computing six-parameter Helmert transformations on the coordinates and velocities of 46 of the 54 core sites used in the ITRF2000 definition. The analysis procedures have been well documented by, for example, *Feigl et al.* [1993], *Dong et al.* [1998], and *Tregoning et al.* [1998]. When combining solutions, we downweighted the vertical components of the GPS data, since we are only interested in horizontal velocities in this study and vertical velocities are known to display significantly non-linear behavior at some sites. The horizontal velocity vectors relative to ITRF2000 are plotted in Figure 2 and listed in Table 2.

3.2. Uncertainty Estimates

[18] When determining the degree of rigidity of a plate it is critical to assign accurate and realistic uncertainties to the estimated station velocities. It is now widely recognized that noise in GPS and other ground deformation data has a red spectrum [e.g., *Langbein and Johnson*, 1997; *Zhang et al.*, 1997; *Mao et al.*, 1999] and that this must be allowed for if uncertainties are to be estimated reliably. This topic is an area of active research, but it is known that the noise spectrum is generally white at high frequencies, and typically between random walk (power spectrum slope of -2) and flicker noise (slope of -1) at low frequencies.

[19] *Johnson and Agnew* [2000], building on earlier work, analyzed the noise characteristics of a >6 year time series of GPS data from a 50-m baseline in southern California. They show for these well-constructed monuments that the long-term instability of physically connecting the GPS antenna and its mount to the surrounding ground displays a random walk characteristic with a stochastic variation of ~0.33 mm^2/yr. Is is well known that any random walk component to the noise will dominate site velocity error estimates once the time series becomes long enough, even in the presence of larger, less-correlated noise sources such as might be induced by reference frame variations [see, e.g., *Wdowinski et al.*, 1997; *Zhang et al.*, 1997]. *Johnson and Agnew* [2000] show that this crossover occurs at remarkably short time series length, less than a year in their California example. Depending on the amplitudes of the random walk components at the GPS stations we have analyzed, these terms may dominate the uncertainty budget for our typically 4–10 year data series.

Table 1. Days per Year of Site Occupations Used in This Analysis

Site	1990	1991	1992	1993	1994	1995	1996	1997	1998	1999	2000	2001	Span[a]
Australian Plate													
ALIC	-	-	-	-	-	25	24	28	179	142	214	251	6
AUCK	-	-	-	-	-	24	89	115	205	161	216	250	6
COCO[b]	-	-	15	12	-	57	77	91	190	107	91	-	8
DARW	-	-	-	1	-	28	8	-	129	68	188	195	8
HOB2	-	-	-	-	2	57	56	89	147	152	215	236	7
KARR	-	-	-	12	-	55	31	4	185	145	202	245	8
NOUM	-	-	-	-	-	-	-	-	210	151	210	233	3
PERT	-	-	-	12	11	68	91	115	213	145	194	105	8
TIDB	-	-	17	26	11	91	93	115	227	149	220	250	9
TOW2	-	-	-	-	-	23	63	36	162	146	220	232	6
YAR1	-	10	27	23	12	101	90	85	228	144	207	205	10
Pacific Plate													
5507	-	-	2	-	-	3	3	4	-	6	5	-	8
5514	-	-	-	1	-	3	-	4	-	-	5	-	7
CHAT	-	-	-	-	-	25	92	116	230	162	221	250	6
FALE	-	-	-	-	-	-	4	4	5	92	91	25	5
KOKB	-	15	21	26	8	95	85	116	228	158	220	247	10
KWJ1	-	-	-	-	-	-	64	116	229	154	104	115	5
MARC	1	-	-	-	-	13	6	4	9	16	6	-	10
MKEA	-	-	-	-	-	-	29	116	203	124	217	251	5
NIUC	-	-	-	-	-	-	2	4	5	15	7	12	5
THTI	-	-	-	-	-	-	-	-	50	46	203	231	3
TRUK	4	-	10	-	5	-	32	65	67	27	-	11	11
WSAM	-	5	-	-	-	-	1	-	2	-	5	-	9
North American Plate													
ALGO	-	10	27	26	12	99	92	114	227	160	219	248	10
BRMU	-	-	-	21	12	99	93	106	218	157	214	229	8
FAIR	-	1	26	26	11	97	93	115	228	129	218	250	10
KELY	-	-	-	-	-	21	58	101	208	146	175	178	6
MDO1	-	-	-	20	12	99	93	113	224	157	210	248	8
NLIB	-	-	-	26	11	99	91	115	227	160	214	238	8
REYK	-	-	-	-	-	-	78	113	200	139	211	244	5
STJO	-	-	18	25	7	97	83	115	227	160	210	246	9
THU1	-	-	-	-	-	57	93	72	202	150	215	111	6
WES2	-	-	-	26	11	92	92	111	221	149	203	212	8
YELL	9	15	28	26	12	99	91	115	227	154	215	237	11
Australian-Pacific Boundary Zone													
5508	-	-	2	1	-	5	-	-	-	3	-	-	7
OUSD	-	-	-	-	-	16	29	31	83	140	109	138	6
WELL	10	15	27	-	-	68	56	-	-	-	-	-	6
WGTN	-	-	-	-	-	-	-	4	5	16	16	13	4
Pacific-North American Boundary Zone													
FARB	-	-	-	-	-	5	12	12	74	74	109	104	6
SCIP	-	-	-	-	-	-	-	-	83	74	31	68	3
SNI1	-	-	-	-	-	-	8	1	69	82	91	100	5
VNDP	-	-	-	-	7	20	16	15	71	95	182	203	7

[a] Time span in years of each time series.
[b] The M_W 7.8 Indian Ocean earthquake of 18 June 2000 caused a 35 mm displacement at station COCO [*Tregoning*, 2002a], so we only use data prior to the earthquake for estimating its velocity.

[20] We therefore take an approach similar to that of *McClusky et al.* [2000] by estimating a combined white noise and random walk noise model and choosing the parameters of this model such that the reduced χ^2 of the overall GPS solution from the GLOBK Kalman filter is approximately unity. (The reduced χ^2 is defined as $\chi^2_\nu = \chi^2/N_{\mathrm{dof}}$, where χ^2 is the weighted residual sum of squares and N_{dof} is the number of degrees of freedom.) In this approach we make the simplification of assuming the same noise model at each station. We then use these velocities and their uncertainty estimates in the Euler vector fitting procedure described in section 4.

[21] We implement the white noise part of the noise model by multiplying the formal errors of the daily network solutions by a scale factor. This is chosen such that when daily solutions are added to the Kalman filter in GLOBK, the increment in χ^2 is on average equal to the increase in N_{dof}. In essence, we are matching the daily error estimates to the short-term repeatability of the coordinate data (which corresponds to the high-frequency end of the noise spectrum). We find that a scale factor of 2 is appropriate for the entire data set. At this stage of the processing we also omit outliers in the data by rejecting any daily coordinate solution for which χ^2/N_{dof} (after

Table 2. Site Codes, Observed ITRF2000 Site Velocities, 1σ Uncertainties, and Residuals

Site	Code	Latitude	Longitude	ITRF2000 Velocity, mm/yr				With Respect to Model		
				V_n	V_e	σ_{V_e}	σ_{V_e}	V_n	V_e	Plate
Australian Plate										
Alice Springs	ALIC	23°40.2′S	133°53.1′E	57.9	31.8	0.6	0.6	0.2	0.1	AU
Auckland	AUCK	36°36.2′S	174°50.1′E	38.6	3.9	0.5	0.5	−0.8	−0.9	AU
Cocos Island	COCO	12°11.3′S	96°50.0′E	49.9	42.1	0.6	0.6	−0.1	−0.7	AU
Darwin	DARW	12°50.6′S	131°08.0′E	57.5	35.4	0.5	0.6	−0.6	−0.3	AU
Hobart	HOB2	42°48.3′S	147°26.3′E	54.8	13.7	0.5	0.5	0.2	−0.4	AU
Karratha	KARR	20°58.9′S	117°05.8′E	57.3	39.3	0.5	0.5	0.2	0.6	AU
Noumea	NOUM	22°16.2′S	166°24.6′E	45.5	20.4	0.7	0.7	0.3	−0.5	AU
Perth	PERT	31°48.1′S	115°53.1′E	57.4	38.7	0.4	0.5	0.5	0.7	AU
Canberra	TIDB	35°24.0′S	148°58.8′E	54.6	18.6	0.5	0.5	0.6	0.3	AU
Townsville	TOW2	19°16.2′S	147°03.3′E	54.2	28.8	0.6	0.5	−0.6	−0.2	AU
Yaragadee	YAR1	29°02.8′S	115°20.8′E	56.1	39.3	0.4	0.5	−0.7	0.7	AU
Pacific Plate										
Auckland Island	5507	50°31.0′S	166°13.7′E	28.1	−29.2	0.6	0.7	0.8	−0.7	PA
Campbell Island	5514[a]	52°32.7′S	169°09.0′E	31.3	−29.5	0.6	0.7	3.0	−2.1	PA
Chatham Island	CHAT	43°57.3′S	176°34.0′W	32.3	−41.2	0.5	0.5	0.5	0.7	PA
Faleolo, Samoa	FALE	13°49.9′S	171°60.0′W	32.2	−64.2	0.7	0.7	−0.3	−0.3	PA
Kokee Park	KOKB	22°07.6′N	159°39.9′W	33.0	−62.6	0.5	0.5	−0.4	0.2	PA
Kwajalein	KWJ1	8°43.3′N	167°43.8′E	27.8	−69.0	0.6	0.6	−0.1	0.6	PA
Marcus Island	MARC	24°17.4′N	153°58.7′E	21.8	−72.3	0.7	0.8	−1.0	−0.6	PA
Mauna Kea	MKEA	19°48.1′N	155°27.4′W	33.4	−63.2	0.6	0.7	0.1	−0.2	PA
Niue	NIUC	19°03.7′S	169°55.9′W	33.3	−63.0	0.7	0.7	0.5	−1.1	PA
Tahiti	THTI	17°34.6′S	149°36.4′W	33.4	−66.5	0.8	0.9	0.5	−0.3	PA
Chuuk	TRUK	7°26.8′N	151°53.2′E	21.8	−69.8	0.5	0.6	−0.1	0.5	PA
Western Samoa	WSAM	13°49.9′S	172°00.9′W	31.8	−64.5	0.7	1.1	−0.7	−0.6	PA
North American Plate										
Algonquin	ALGO	45°57.3′N	78°04.3′W	2.1	−16.3	0.5	0.4	−0.2	0.4	NA
Bermuda	BRMU	32°22.2′N	64°41.8′W	8.2	−12.1	0.4	0.4	0.9	0.3	NA
Fairbanks	FAIR[a]	64°58.7′N	147°30.0′W	−21.5	−8.6	0.4	0.4	−1.8	0.9	NA
Kangerlussuaq	KELY	66°59.2′N	50°56.7′W	11.2	−16.9	0.6	0.6	−0.8	0.7	NA
McDonald Obs.	MDO1	30°40.8′N	104°00.9′W	−7.1	−12.3	0.4	0.5	0.4	−0.5	NA
North Liberty	NLIB	41°46.3′N	91°34.5′W	−2.3	−14.9	0.5	0.5	0.6	0.7	NA
St. John	STJO	47°35.7′N	52°40.7′W	12.0	−15.1	0.4	0.5	0.6	−0.2	NA
Thule	THU1	76°32.2′N	68°47.3′W	4.6	−22.2	0.5	0.5	−1.2	−1.2	NA
Westford	WES2	42°36.8′N	71°29.6′W	3.9	−16.3	0.4	0.5	−0.8	−0.7	NA
Yellowknife	YELL	62°28.9′N	114°28.8′W	−11.1	−17.5	0.4	0.4	0.1	0.0	NA
Australian-Pacific Boundary Zone										
Christchurch	5508	43°34.9′S	172°44.6′E	30.8	−35.4	0.7	0.8	1.4	2.9	PA
Dunedin	OUSD	45°52.2′S	170°30.7′E	30.4	−32.1	0.5	0.5	1.6	3.0	PA
Wellington	WELL	41°16.5′S	174°47.0′E	33.3	−21.4	0.8	0.9	−6.1	−21.6	AU
Wellington Airport	WGTN	41°19.4′S	174°48.4′E	31.4	−24.4	0.7	0.8	−8.0	−24.5	AU
Pacific-North American Boundary Zone										
Farallon Island	FARB	37°41.8′N	123°00.0′W	25.1	−41.3	0.5	0.6	−1.8	0.3	PA
San Clemente Island	SCIP	32°54.9′N	118°29.3′W	22.5	−42.2	0.7	0.8	−2.8	2.9	PA
San Nicolas Island	SNI1	33°14.9′N	119°31.5′W	22.0	−42.4	0.6	0.6	−3.6	2.6	PA
Vandenberg AFB	VNDP	34°33.4′N	120°37.0′W	22.3	−42.8	0.5	0.5	−3.7	1.2	PA

[a] Not used in Euler vector fit.

scaling) is >10. Less than 1% of daily solutions are rejected in this manner.

[22] We implement the random walk part of the model by including a random walk component in the GLOBK noise model, as described by *McClusky et al.* [2000]. We find that a random walk amplitude of 1 mm/$\sqrt{}$yr on each of the north and east components gives an overall χ^2_ν of unity for the GLOBK solution.

[23] The uncertainties derived from this noise model behave in a ''sensible'' fashion. Uncertainties decrease slowly with the length of the time series, and also decrease very slowly with the number of samples in the time series. In other words, data span is more important than high temporal density of samples in reducing the velocity uncertainty. This justifies our strategy of not always analyzing daily data, but rather analyzing the longest possible time span at each station.

4. Euler Vector Estimation

4.1. ITRF2000 Euler Vectors

[24] We generate rigid plate models by calculating a single Euler vector that best fits the velocities in the interior of various plates. We estimate Euler vectors relative to ITRF2000 for AU, PA, and NA separately (Table 3), initially using all available site velocities on each plate. The estimation is an overdetermined least squares problem for which we carry the full covariance matrix through the inversion.

Table 3. Euler Vectors for Australian, Pacific, and North American Plates[a]

Euler Vector	Latitude	Longitude	Rate, deg/Myr	Pole Error Ellipse			χ^2_ν
				σ_{maj}	σ_{min}	Azimuth	
			Pacific Plate				
PA - this paper (ITRF2000)	−63.75	110.86	0.677 ± 0.002	0.61	0.15	85	0.93
Tregoning [2002b] (ITRF97)	−64.3	114.2	0.649 ± 0.005	1.6	0.4	82	
Tregoning et al. [1998] (ITRF94)	−61.4	105.0	0.63 ± 0.01	2.8	1.1	54	
NNR-1A[b]	−63.0	107.4	0.64	-	-	-	
			Australian Plate				
AU - this paper (ITRF2000)	32.76	37.54	0.621 ± 0.002	0.40	0.13	109	1.08
Tregoning [2002b] (ITRF97)	35.1	36.5	0.619 ± 0.004	0.8	0.3	107	
Tregoning et al. [1998] (ITRF94)	31.6	41.3	0.62 ± 0.01	2.9	1.4	113	
NNR-1A[a]	33.8	33.2	0.65	-	-	-	
			North American Plate				
NA - this paper (ITRF2000)	−3.86	−83.96	0.199 ± 0.003	1.02	0.41	4	1.47
NNR-1A[b]	−2.4	−85.9	0.207	-	-	-	
			Pacific-Australia				
PA/AU - this paper	−61.04	184.19	1.078 ± 0.004	0.37	0.17	82	
Tregoning [2002b]	−60.9	184.9	1.077 ± 0.008	0.8	0.5	82	
Tregoning et al. [1998]	−61.4	186.8	1.01 ± 0.02	2.4	2.3	84	
Larson et al. [1997]	−65.7	182.9	1.04 ± 0.02	1.7	1.5	2	
Spitzak and DeMets [1996][c]	−60.7	185.2	1.11 ± 0.01	0.8	0.6	130	
NUVEL-1A, *DeMets et al.* [1994]	−60.08	181.74	1.074 ± 0.01	1.0	0.9	58	
			Pacific-North America				
PA/NA - this paper	50.26	284.96	0.773 ± 0.005	0.41	0.17	94	
DeMets and Dixon [1999] GPS	51.5	286.3	0.765 ± 0.016	2.0	1.0	95	
Larson et al. [1997]	49.6	275.7	0.83 ± 0.02	2.0	1.0	94	
NUVEL-1A, *DeMets et al.* [1994]	48.7	281.8	0.75 ± 0.01	1.3	1.2	119	

[a] Rotation is in a clockwise direction about the Euler vector of the first-named plate relative to the second. The uncertainty ellipses of the poles are described by the 1σ semimajor and semiminor axes of each ellipse and the clockwise angle from true north of the semimajor axis. For our Euler vector estimates the uncertainties have not been scaled by the separate $\sqrt{\chi^2_\nu}$ for each individual model, but the value of χ^2_ν is given in the table to show the goodness of fit for each model.

[b] No-Net-Rotation-Nuvel-1A (NNR-1A) model [*Argus and Gordon*, 1991; *DeMets et al.*, 1994]. These are only directly comparable to the geodetically-derived Euler vectors insofar as the ITRF realizations are no-net-rotation frames aligned with NNR-1A [see *Zhang et al.*, 1999].

[c] We scaled *Spitzak and DeMets'* [1996] rate by 0.9562 to adjust from the NUVEL-1 to NUVEL-1A timescale [*DeMets et al.*, 1994].

[25] We then evaluate the goodness of fit of the velocities to the plate model. If our noise model significantly underestimated the velocity uncertainties, we would find $\chi^2_\nu \gg 1$. If it overestimated the uncertainties we would find $\chi^2_\nu \ll 1$. (If the plates were not completely rigid we would also expect χ^2_ν to be >1.) In fact, with our chosen noise model we find χ^2_ν between 0.9 and 1.5 for each of the Pacific, Australian, and North American plates. This suggests that our noise model is reasonable and that our estimated standard errors are correct to ∼20%.

[26] Since our velocity uncertainties were estimated from the overall GPS solution independently of the quality of the fit of the velocities to a rigid plate model, we may use the goodness of fit of the velocities to the plate model to provide information about plate rigidity. We therefore do not scale the uncertainty estimates for Euler vector fits to the individual plates by the $\sqrt{\chi^2_\nu}$ value for each fit. Instead, we report each value of χ^2_ν in Table 3 as an indication of the goodness of fit of each model. We note that all uncertainty estimates quoted in the text are ±1σ unless otherwise noted.

4.1.1. Australian Plate

[27] For AU alone we find that the reduced χ^2 of the fit is 1.08. The RMS of the velocity residuals is 0.4 mm/yr and the greatest deviation from the model in any component is −0.9 ± 0.5 mm/yr (Figure 3 and Table 2), showing that the Australian Plate is rigid at this level all the way from Cocos Island in the northwest, to Tasmania in the south and to New Caledonia and Auckland in the east, as previously demonstrated by *Tregoning* [2002b]. We experimented with estimating the Euler vector from subsets of the 11 stations but could find no evidence that any stations were outliers.

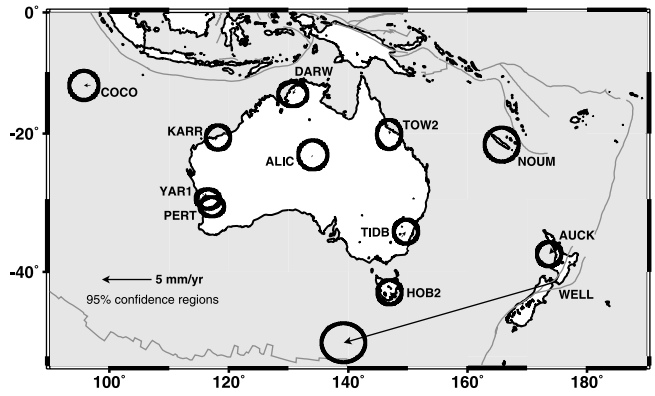

Figure 3. Residual GPS velocities at Australian Plate stations with 95% confidence uncertainty ellipses. The residual velocity for station WELL is shown, though this station is, of course, not included in the plate fit.

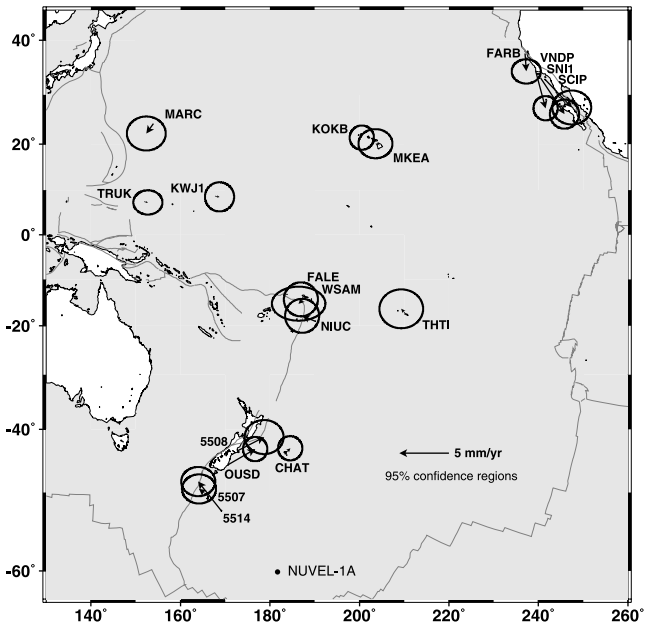

Figure 4. Residual GPS velocities at Pacific Plate stations with 95% confidence uncertainty ellipses. Station 5514 is not included in the plate fit. The position of the NUVEL-1A AU/PA relative pole is shown for reference.

Our estimate for the AU Euler vector is statistically indistinguishable from the earlier estimate of *Tregoning* [2002b], even though longer time series have been used in the present solution.

[28] We include in Table 2 the velocity estimates and residuals with respect to AU for two sites in Wellington, which is nominally on the Australian Plate. This is partly for historical interest because the velocity of one of these sites (WELL) was also reported by *Larson et al.* [1997] and partly because these velocities are of interest to regional studies of interplate motion in New Zealand [e.g., *Darby and Beavan*, 2001].

4.1.2. Pacific Plate

[29] Using all 12 stations that are located on the interior of PA (at 11 independent sites, since WSAM and FALE are nearly colocated) we find that the velocity of station 5514 is an outlier, with a residual of greater than 4 standard errors. Removing this station from the fit we find that the reduced χ^2 is 0.9, the RMS residual is 0.4 mm/yr, and the greatest deviation from the model is 1.1 ± 0.7 mm/yr (Figure 4 and Table 2). These values are very similar to the corresponding values for the Australian Plate.

4.1.3. North American Plate

[30] For NA we have nine velocities available, all of which are in common with the 10 stations used by *Kogan et al.* [2000], and eight of which are in common with the 16 stations of *DeMets and Dixon* [1999]. Though *DeMets and Dixon* [1999] use a large number of stations, our time series are much longer than the 2.5–4 years available to these authors. We have not corrected our station velocities for ongoing deformation due to glacial isostatic adjustment (GIA), since we show below that these effects have an insignificant effect on the NA Euler vector. We find that the reduced χ^2 of the fit is 1.47, the RMS of the residuals is 0.6 mm/yr, and the greatest deviation from the model is −1.2 ± 0.5 mm/yr (Figure 5 and Table 2). These values place a similar constraint on North American Plate stability as *DeMets and Dixon*'s [1999] values (0.8 mm/yr, 1.7 ± 1.2 mm/yr) or *Kogan et al.*'s [2000] values these authors' (0.6 mm/yr, 1.4 ± 1.0 mm/yr), where we have calculated RMS and greatest deviation values using only their stations that are in common with ours.

[31] We did not use station FAIR in our NA plate fit because earlier work of *Ma et al.* [1990] and *Kogan et al.* [2000] indicates that FAIR should not be considered on the rigid North American Plate. Our analysis (Table 2) confirms a small but significant (>4 standard errors) residual of 2.0 ± 0.4 mm/yr at 153° ± 12°. However, our residual is much smaller than *Kogan et al.*'s [2000] GPS estimate of 5.0 ± 0.8 mm/yr at 125° ± 10°, and is more in line with *Ma et al.*'s [1990] VLBI estimate of 1.5 ± 0.5 mm/yr at 168° ± 20°.

[32] The fact that the misfit to NA is worse than the misfits to either AU or PA could imply internal deformation of the North American Plate. One recognized source of such deformation is isostatic adjustment following the Laurentide glaciation [e.g., *Peltier*, 1994]. To investigate this we have estimated an NA Euler vector that includes corrections to our observed velocities using the GIA velocities quoted by *Kogan et al.* [2000] based on the ICE-4G model of *Peltier* [1994]. We find that the fit is improved by ~10% when the ICE-4G GIA corrections are included. This improvement indicates that GIA may be one cause of the higher residuals on NA and implies that newer GIA models may improve the fit still further, to perhaps approach the same levels found for PA and AU. (We note that we omitted station KELY in Greenland from the GIA comparison since there is evidence that this station is responding to recent advance of the western ice sheet margin [*Wahr et al.*, 2001].) Even when

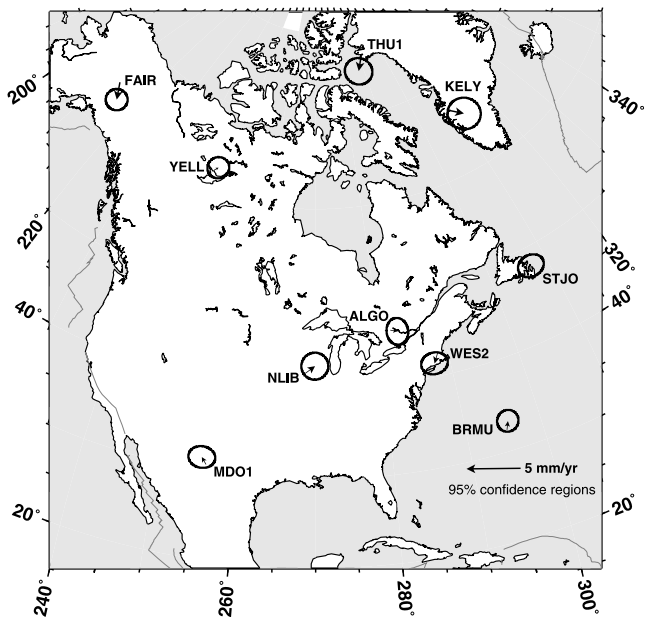

Figure 5. Residual GPS velocities at North American Plate stations with 95% confidence uncertainty ellipses. Station FAIR is not included in the plate fit.

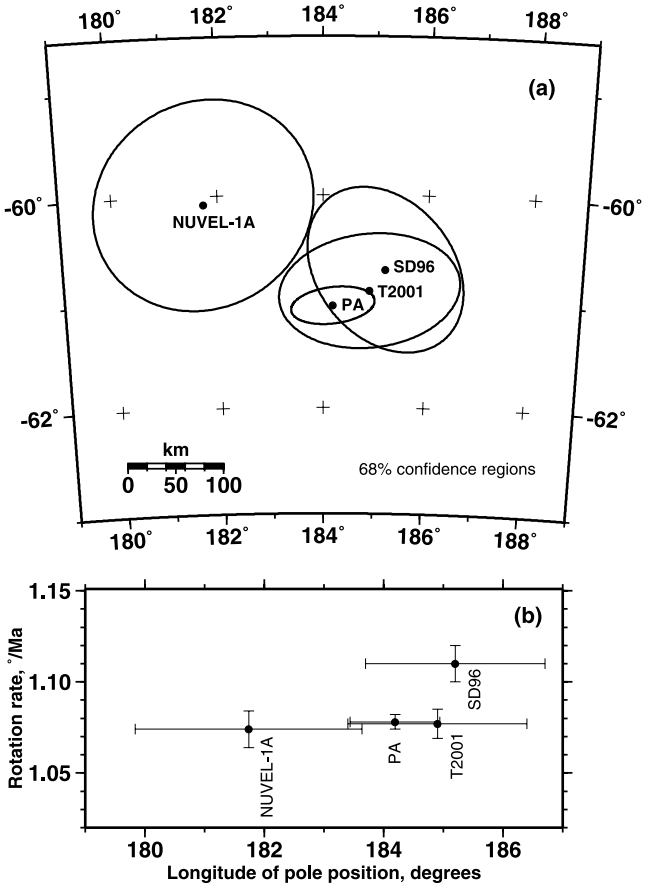

Figure 6. (a) Various estimates of the PA/AU pole position with 68% confidence regions. PA refers to this study, SD96 to *Spitzak and DeMets* [1996], and T2001 to *Tregoning* [2002b]. (The *Larson et al.* [1997] pole is located at 65.7°S, several degrees off the bottom of the map.) (b) Estimated rotation rate for each pole plotted against longitude. The error bars are the 1σ rate errors and the 68% confidence longitude errors. PA is statistically indistinguishable from T2001, its difference from NUVEL-1A is not significant at the 95% confidence level, and its difference from SD96 is barely significant at the 95% confidence level.

we include the ICE-4G GIA corrections, the derived Euler vector changes insignificantly, with the NA/PA pole position moving by <30 km and the rotation rate changing by <0.3%. We have therefore not used GIA corrections for estimating NA Euler vectors in the present paper.

4.2. Relative Euler Vectors

[33] We calculate relative Euler vectors by simultaneously fitting the AU, NA, and PA station velocities. Our results are shown in Table 3, where they are compared with some previous space-geodetic and geological estimates. Our PA/AU Euler vector (see also Figure 6) is not statistically distinguishable from *Tregoning*'s [2002b] estimate even though we use nearly twice as many stations. However, the confidence limits on our results are substantially improved over previous estimates. Our PA/NA Euler vector is not statistically distinguishable from *DeMets and Dixon*'s [1999] estimate. The *Larson et al.* [1997] relative poles are clearly different in both cases, presumably as a result of their limited Pacific Plate data discussed earlier.

[34] In Table 4 we show the predictions of various models for the right-lateral strike-slip and shortening rates along and across the plate boundary at two locations in central South Island. These locations are near the northern and southern extents of the plate boundary-crossing GPS network discussed by *Beavan et al.* [1999]. In comparison with NUVEL-1A, all models except that of *Larson et al.* [1997] predict modestly faster fault-parallel rates and the same or modestly slower shortening rates.

5. Discussion

5.1. Rigidity of the Pacific Plate Interior

[35] The portion of the Pacific Plate interior that we have sampled with our measurements appears approximately as rigid as the Australian Plate, with each showing RMS velocity residuals of 0.4 mm/yr to a rigid plate model. The North American Plate appears somewhat less rigid, with RMS residuals of 0.6 mm/yr that may in part be due to unmodeled effects of glacial isostatic adjustment. We do not find that the oceanic Pacific Plate is significantly more rigid than the continental Australian Plate. This may be because the station velocity errors are dominated by sources other than plate rigidity, which means that our value of 0.4 mm/yr RMS is only an upper limit on the true stability of the plate interiors.

5.2. Stability of GPS Stations

[36] Since station 5514 is a clear outlier and since there have been previous indications that CHAT may be moving relative to the Pacific Plate [*DeMets and Dixon*, 1999; *Tregoning*, 2002b], we investigate whether there is any evidence of local instability or erroneous measurements at these two stations.

[37] The CHAT monument consists of a reinforced concrete pillar extending 0.8 m above ground. The pillar is founded in a 0.3 m thick, very firm layer near the top of a 30 m soil sequence derived from Eocene tuff, which lies above basement probably consisting of late Cretaceous extrusive volcanics [*Campbell et al.*, 1993; N.Z. Seismological Observatory, unpublished drill log, 1973]. Because the site

Table 4. Interplate Velocities Evaluated at the Alpine Fault[a]

	Fox Glacier, 43.5°S, 170.0°E		Harihari, 43.15°S, 170.5°E	
Euler Vector	V_{rl}	$V_{contrac}$	V_{rl}	$V_{contrac}$
PA/AU this paper	38.9 ± 0.4	9.1 ± 0.6	39.1 ± 0.4	9.8 ± 0.6
Tregoning [2002b]	39.2 ± 1.1	8.4 ± 1.5	39.4 ± 1.1	9.1 ± 1.5
Tregoning et al. [1998]	38.6 ± 4.5	7.3 ± 4.6	38.8 ± 4.5	8.0 ± 4.6
Larson et al. [1997]	42.9 ± 3.4	16.1 ± 3.0	43.1 ± 3.4	16.8 ± 3.0
Spitzak and DeMets [1996]	40.3 ± 1.6	8.1 ± 1.5	40.5 ± 1.6	8.9 ± 1.5
NUVEL-1A	35.7 ± 1.9	9.5 ± 2.0	36.0 ± 1.9	10.3 ± 2.0

[a] Velocities are in mm/yr. V_{rl} is the right-lateral velocity parallel to the Alpine Fault, $V_{contrac}$ is the horizontal shortening rate normal to the fault. For comparison, the interplate velocities inferred by *Beavan et al.* [1999] from a South Island crossing GPS network located between Fox Glacier and Harihari are 39.0 ± 1.5 mm/yr right-lateral and 10.5 ± 1.5 mm/yr horizontal shortening.

Table 5. Days of Occupation of Chatham Island Station Ties

Baseline	Length	1992	1995	1997	1998	1999	2001
CHAT to 5503	54 m	-	3	1	2	1	2
CHAT and/or 5503 to 5504	16.8 km	4	1	-	-	-	2

conditions are not ideal, CHAT has been tied on several occasions to two preexisting reference marks at distances between 50 m and 17 km (Table 5). The nearby mark, 5503, is in the same ground conditions as CHAT, while the more distant mark, 5504, is in ground that appears substantially more stable than at CHAT, with bedrock occurring at only a few meters depth.

[38] CHAT has been very stable relative to 5503 (<0.3 mm/yr change over 5.5 years), showing there are no significant local instabilities in the immediate vicinity of the CHAT monument. Similarly, the motion between CHAT and the more distant mark, 5504, has been <0.5 mm/yr over 5.5 years, showing that there has also been no significant regional instability. Any local or regional instability at CHAT is therefore at about the noise level of our velocity estimates.

[39] Station 5514 is a bronze survey disk concreted into bedrock at the summit of a low hill and there is no reason to suspect local instability. There are also no obvious outliers in the position time series. One possible source of unusual motion at this site could be postseismic effects of the great Macquarie Ridge earthquake of 1989 [*Ekstrom and Romanowicz*, 1990; *Satake and Kanamori*, 1990]. We have generated several models using the code of *Pollitz* [1997] and a variety of mantle viscosity structures. We find that the predicted velocities range from a couple of millimeters per year (using an unrealistically low mantle viscosity of 10^{18} Pa s) to insignificant, that they are always directed between south and southwest (orthogonal to the observed residual), and that the modeled velocity is always at least twice as large at station 5507 than it is at 5514. We therefore rule out the Macquarie earthquake as a source of the anomalous velocity at 5514, which remains unexplained.

5.3. Deformation at Plate Boundaries

[40] What are the implications of the PA predicted motions at the AU/PA boundary in New Zealand and at the PA/NA boundary in California? For the coastal and offshore southern California stations, VNDP, SCIP, and SNI1, the velocities with respect to the PA predictions are 4–5 mm/yr, while in northern California the residual velocity at FARB is only ~2 mm/yr (Figure 7a). The residual velocities with respect to PA predicted motions at OUSD and 5508 on the east coast of the South Island are ~3 mm/yr (Figure 7b). It is at first sight surprising that most of these residuals are so large, since many previous researchers have implicitly or explicitly assumed that the offshore sites in California [e.g., *Freymueller et al.*, 1999] and the eastern sites in South Island [e.g., *Pearson et al.*, 2000] are moving at close to Pacific Plate velocity, where "close" has been thought of as less than 2–3 mm/yr rather than 3–5 mm/yr.

[41] It is important to note that the residuals in California and South Island are not only correlated with each other within each region but are also directed nearly opposite to the direction of interplate motion at those sites. This strongly suggests that the residuals are related to the plate boundary tectonics rather than any other effect. Furthermore, because the residual velocities offshore of New Zealand and California are nearly orthogonal to each other, there is no rotation of PA that can simultaneously reduce the residuals by a significant amount in both California and New Zealand.

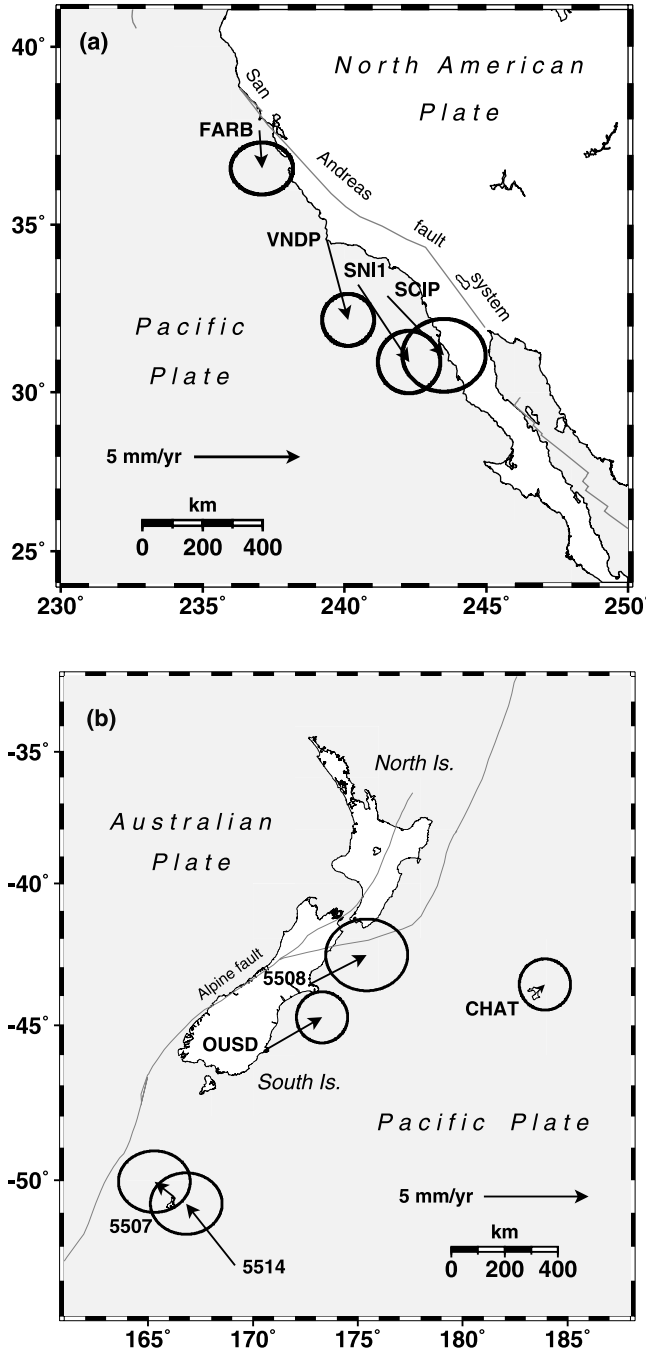

Figure 7. (a) Residual GPS velocities at California coastal and offshore stations with respect to the PA Euler vector, with 95% confidence uncertainty ellipses. (b) Residual GPS velocities at New Zealand coastal and offshore stations with respect to the PA Euler vector, with 95% confidence uncertainty ellipses.

The implication is that there is substantially more present-day deformation than previously believed offshore of both California and New Zealand. Perhaps the plate boundary zones are wider than previously suspected?

[42] The long-term rates of motion of stations near the plate boundary may be estimated from geological evidence if all active faults in the region have been identified and their long-term slip rates estimated. Present-day velocities (and velocity deficits relative to the plate interior) may be estimated from models of strain accumulation along the known plate boundary faults. In the next three sections we examine the evidence for offshore deformation then attempt to model our observations as elastic strain accumulation.

5.3.1. Deformation Offshore of South Island

[43] Several lines of evidence show that stations 5508 and OUSD are not moving with rigid Pacific Plate velocity, at least at the present time. OUSD is located in the widest part of the South Island continental collision zone, where the active deformation front lies some 20 km offshore to the east. There are many faults mapped from reflection profiling between the coast and the deformation front. Those studied in detail [*Johnstone*, 1990] are mapped as reverse faults but there is no way to rule out a component of strike slip motion. Uplifted marine terraces associated with the partially onshore Akatore Fault east of OUSD have been studied using paleoseismological techniques [*Litchfield and Norris*, 2000]. The Akatore Fault underwent a clear ~3 m uplift event ~1100 years ago, and another similar event tentatively dated at ~4000 years ago, though it seems that this particular fault was quiescent for the preceding 80,000 years. The estimated long-term shortening rate normal to the fault is 0.5–1 mm/yr, and there is slickenside evidence of a small component of right lateral motion. Also, first motions of the M_L = 5.0 Dunedin earthquake of 1970 are consistent with predominantly right lateral strike-slip on a ENE striking fault plane [*Adams and Kean*, 1974]. However, we have insufficient knowledge of right-lateral faulting in this region to be able to say whether a ~3 mm/yr residual can be accounted for by slip on regional faults.

[44] There is no evidence of significant active faulting east of station 5508. However, there are a number of active faults to its west and elastic strain accumulation associated with these will cause the present-day velocity of 5508 to be less than Pacific Plate velocity even if 5508 moves with the Pacific in the long term. *Beavan and Haines* [2001] have estimated the present-day velocities of GPS stations throughout New Zealand and their results indicate that 5508 is moving at least 3 mm/yr east-northeasterly relative to their representation of the Pacific Plate. This is in the same direction and at a similar rate as the residual derived here.

5.3.2. Deformation Offshore of California

[45] There are no reports of active faults west of FARB in California but there is an extensive network of active faults to the east, with the San Andreas Fault only 35 km away. Elastic strain accumulation associated with these faults will cause FARB to move slower than Pacific Plate velocity during an interseismic period.

[46] *Freymueller et al.* [1999] calculate a velocity field in northern California from an east-west transect of GPS sites and use it to estimate fault slip rates and locking depths across the plate boundary. They define a velocity field relative to the "Pacific Plate" by adopting a Pacific-referenced velocity at the Point Reyes National Crustal Measurement Network (NCMN) site of 7 ± 2 mm/yr, taken from the VLBI estimate of *Ma et al.* [1995]. (Point Reyes NCMN is located some 50 km north of FARB, or ~30 km in a plate boundary-normal direction.) *Freymueller et al.* [1999] support this estimate by assuming FARB is fixed to the Pacific Plate and using regional GPS and electronic distance measurement (EDM) data which imply 7.7 ± 2.5 mm/yr right-lateral relative motion between FARB and Point Reyes NCMN. The agreement between these two estimates appears to support *Freymueller et al.*'s [1999] assumption that FARB is Pacific fixed, but we note that *Ma et al.*'s [1995] Pacific reference frame relies on very few stations in the Pacific interior, all of them grouped in the western Pacific from Hawaii westward.

[47] Our PA estimate of the velocity deficit of FARB relative to the Pacific Plate is 1.8 ± 0.8 mm/yr at an azimuth of 169°. This implies a Pacific-fixed velocity of 9.3 ± 2.6 mm/yr at Point Reyes NCMN, some 2–3 mm/yr higher than the value adopted by *Freymueller et al.* [1999]. *Freymueller et al.*'s [1999] reference velocity is based on an assumption that FARB is Pacific fixed, and much of their analysis is based on this premise. However, they also present an alternate solution (in their Table 5) in which they allow a ±2 mm/yr uncertainty in their Pacific reference frame. This leads to a higher overall right-lateral velocity across the plate boundary (41.1 versus 39.6 mm/yr with error estimates on the order of ±1 mm/yr) and a deeper locking depth on the San Andreas (18.2 versus 14.9 km, though with wide error estimates on the order of 10 km). Our results suggest that their alternate reference frame is more appropriate, implying the higher 41.1 mm/yr rate across the Northern California part of the plate boundary. However, additional unrecognized low slip-rate faults west of the San Andreas could also contribute to the velocity we observe at FARB.

[48] In southern California, there are no major active faults mapped west of stations VNDP and SCIP, but it is possible that such faults exist (Figure 1b). SNI1 is farther offshore than the other two stations and is therefore the station most likely to be moving with full Pacific Plate velocity. All these stations will be affected to a greater or lesser degree by elastic strain accumulation on active faults to their east, as investigated more fully in section 5.3.3.

5.3.3. Predicted Relative Motion From Dislocation Models

[49] In Figure 8 we show cross sections of the active plate boundary strike-slip fault networks in the vicinity of the GPS stations, with long-term slip rates and locking depths indicated for each fault. We assume an elastic half-space with each fault slipping at its long-term rate below the locking depth. For simplicity we assume the faults are infinitely long and sum the analytic solution [*Savage and Burford*, 1973] for each fault to calculate the velocity deficit at each GPS station. In Table 6 we compare the model deficits with the observed residuals to PA.

[50] At FARB the predicted velocity deficit from elastic strain accumulation is close to the observed residual. For the South Bay profile the predicted deficit exceeds the FARB residual, but since FARB lies closer to the North Bay profile it is fairer to compare with this profile. Here the predicted

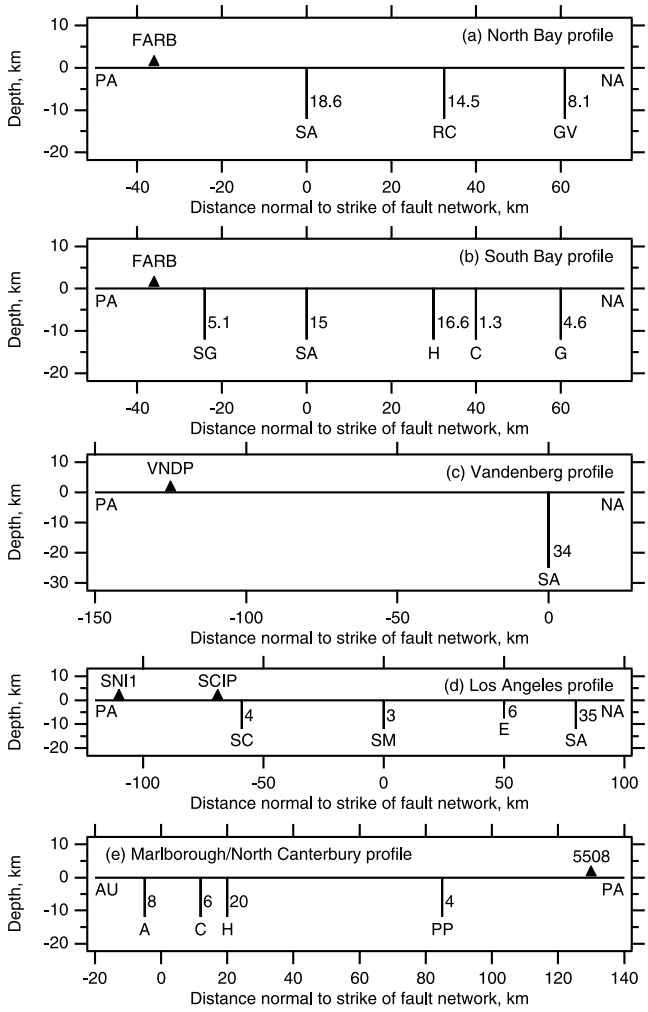

Figure 8. Idealized cross sections normal to the plate boundary strike-slip fault networks in (a and b) the San Francisco Bay area, (c) the Vandenberg area, (d) the Los Angeles area just north of the San Jacinto/San Andreas junction, and (e) the southern Marlborough/North Canterbury region of New Zealand. Faults are SA, San Andreas and in Figure 8a, RC, Rogers Creek; GV, Green Valley; Figure 8b, SG, San Gregorio; H, Hayward; C, Calaveras; G, Greenville; Figure 8d, SC, San Clemente; SM, Sierra Madre; E, Elsinore; Figure 8e, A, Alpine; C, Clarence; H, Hope; PP, Porter's Pass. Adjacent to the faults are their estimated long-term slip rates from *Savage et al.* [1999] (Figures 8a and 8b), *Feigl et al.* [1993] (Figure 8c) (there are undoubtedly active faults west of the San Andreas missing from this idealization), *Bennett et al.* [1996] (Figure 8d), and *Bourne et al.* [1998] (Figure 8e). We have added to those given by *Bourne et al.* [1998] the developing Porter's Pass fault zone, which is estimated to have a slip rate between 2.7 and 5 mm/yr [*Berryman*, 1979; *Knuepfer*, 1992]. Also shown are the positions of GPS stations relative to the fault networks. See Table 6 for the estimated velocities of the GPS stations relative to the plate interior due to elastic strain accumulation on these faults.

deficit is 2.0 mm/yr faster than the observed PA residual if the locking depth is taken as 15 km, or 0.8 mm/yr faster for a locking depth of 10 km. We think that these mismatches are reasonable given the various errors involved, so that the velocity of FARB is consistent with our PA Euler vector, particularly for the model with 10 km locking depth on the plate boundary faults.

[51] For VNDP we used the fault slip model of *Feigl et al.* [1993]. From maps on the SCEC web site (http://www.scecdc.scec.org/group_e/release.v2/fig3.html) it appears there are other active faults between VNDP and the San Andreas (as well as possible active faults offshore), but we know of no study that has estimated slip rates on these faults. The fact that the predicted velocity deficit at VNDP is some 2 mm/yr smaller than the observed residuals to PA could perhaps be explained if these faults were included in the model.

[52] SCIP lies west of all the major mapped faults but is close to the San Clemente Fault. The predicted velocity deficit is ~1.5 mm/yr slower than the PA residual if the locking depth is 15 km, reducing to <1 mm/yr discrepancy if the slip rate on the San Clemente Fault is increased to 6 mm/yr.

[53] SNI1 lies well west of all the major mapped faults, and the fact that this station also has a high residual to PA is what most requires explanation. The predicted velocity deficit is only 1.2 mm/yr while the observed residual is 4.5 mm/yr, even higher than the SCIP and VNDP residuals. We cannot explain this discrepancy other than by postulating a local source of deformation or instability near SNI1, or additional faults farther offshore. The fact that the velocities at the California borderland stations are highly correlated argues to some extent against the instability hypothesis.

[54] Our results suggest that the continental crust bordering parts of the Pacific Plate deforms much more significantly than the oceanic interior of the plate. One mechanism that can make plate boundary strain fields wider than expected from an elastic half-space model is viscoelastic flow within the lower crust or asthenosphere. *Savage and Lisowki* [1998] show that late in an interseismic period the apparent depth of locking can be as much as three times the

Table 6. Velocity Deficits at Offshore Stations Predicted From Plate Boundary Fault Models[a]

Station	Profile	Locking Depth	V_{pred}	V_{res}
FARB	North Bay	10 km	2.6	1.8 ± 0.8
		15 km	3.8	1.8 ± 0.8
	South Bay	10 km	3.5	1.8 ± 0.8
		15 km	5.0	1.8 ± 0.8
SCIP	LA	10/7.5 km[b]	2.2	4.0 ± 1.1
		15 km	2.7	4.0 ± 1.1
SNI1	LA	10/7.5 km[b]	1.2	4.5 ± 0.9
		15 km	1.5	4.5 ± 0.9
VNDP	Vandenberg	25 km	2.1	3.9 ± 0.7
5508	Marl./No. Cant.	15 km	1.8	3.2 ± 1.1

[a] V_{pred} is the velocity deficit predicted by an elastic dislocation model using estimated slip rates and locking depths on known plate boundary faults. V_{res} is the velocity residual to the PA Euler vector model. Slip rates and locking depths are from *Savage et al.* [1999] for North and South Bay networks, *Bennett et al.* [1996] for LA network, *Feigl et al.* [1993] for Vandenberg region, and *Bourne et al.* [1998] for Marlborough/North Canterbury (Marl./No. Cant.) network. Station OUSD is not included because fault-slip rates near this site are not well known.

[b] Variable locking depths as from *Bennett et al.* [1996]. See Figure 8d.

elastic layer thickness for an end-member model consisting of an elastic layer over a viscoelastic half-space. While the effect would be smaller in a more realistic model, this mechanism may provide a partial explanation for the large residuals we observe at VNDP and SCIP. However, we do not believe the effect can be large enough to explain the residuals at stations 5508 or SNI1. *Dixon et al.* [2000] have independently come to similar conclusions about site SNI1 and have made a quantitative estimate of the viscoelastic coupling effect at that site.

[55] An alternative explanation of the large residuals we observe at the Channel Island sites in southern California could be pervasive deformation of the Pacific Plate between Hawaii and California (though there is no obvious evidence for such deformation). The collection of GPS data on oceanic islands well offshore of Mexico (G and R in Figure 1a) would provide a way of differentiating between these possibilities (and we note that a continuous GPS station was established at Isla Guadalupe in early 2001). Under the first scenario, G and R will be moving at essentially the velocity predicted by our PA model, while under the alternative explanation their velocities will be close to the velocities of the Channel Island stations.

5.3.4. Deformation Across South Island

[56] The PA/AU model makes predictions that are consistent with other evidence both for shortening across South Island, and for plate boundary-parallel shear across the island (Table 4). *Beavan et al.* [1999] have recently shown that the velocity predicted by the *Larson et al.* [1997] PA/AU Euler vector is significantly too high compared to the velocity field across South Island determined from regional GPS campaigns, but they were unable to discriminate between other models. Meanwhile, in part because of the disagreement between the NUVEL-1A and *Larson et al.* [1997] estimates, *Walcott* [1998] used a 6.4 Myr average rate of 13 mm/yr in his discussion of South Island tectonics, which he derived from the finite rotation of anomaly 3a using the satellite gravity data of *Cande et al.* [1995] and the *Cande and Kent* [1995] timescale.

[57] Our new and more precise PA/AU Euler vector predicts a present-day Alpine fault-parallel interplate velocity of 38.9 ± 0.4 mm/yr and fault-normal shortening rate of 9.1 ± 0.6 mm/yr at latitude 43.5°S. This provides excellent boundary conditions for studies of deformation within the New Zealand plate boundary zone, one of which is described briefly in section 5.3.5.

5.3.5. Implications for Continental Collision in South Island

[58] *Batt and Braun* [1999] use a fully thermally coupled dynamical model of the evolution of the Southern Alps compressional orogen and predict the distribution of apparent ages of a variety of isotopic systems, which they compare with a large body of newly collected and preexisting isotopic age data. They test the observed isotopic age distribution against three models of collision that have each been supported by various forms of evidence over the past few years. In all the models, there is slow convergence at 2 mm/yr from 10 to 5 Ma. In one model the rate remains steady at 10 mm/yr following a rapid major plate reorganization at about 5 Ma, in the second the rapid increase in convergence rate does not occur until about 1.3 Ma, while in the third they allow a steady increase of rate from 2 mm/yr at 5 Ma to 10 mm/yr at present. Their geochronological data favor a steady shortening rate since 5 Ma, which is also supported by the similarity of our present-day PA/AU Euler vector and the 3-Ma averages of *DeMets et al.* [1994] and *Spitzak and DeMets* [1996] (see also section 5.4).

5.4. Stability of Plate Motions

[59] Our present-day PA/NA Euler vector agrees closely with that of *DeMets and Dixon* [1999], so we concur with those authors on the stability of PA/NA motion over the past 3 Myr. We also agree with them that the PA/NA relative motion in the western United States is some ~4 mm/yr faster than predicted by NUVEL-1A.

[60] We find that our present-day PA/AU pole is located some 170 km southeast of the NUVEL-1A pole with a very similar rotation rate (Table 3 and Figure 6). However, the difference between the Euler vectors is not significant at the 95% confidence level. *Spitzak and DeMets* [1996] have used Seasat and Geosat satellite altimetry data to collect a much larger amount of information from Southern Ocean plate boundaries than was used in the NUVEL-1A model. Their PA/AU pole position lies only 70 km from our PA/AU pole, but their rotation rate is ~3% faster than ours, with the difference between the Euler vectors barely significant at the 95% confidence level. Given the similarity between our present-day estimate and the geologically-based estimates, we infer that the PA/AU pole position has been essentially stable over the past 3 Myr and that the rate has probably also been stable and certainly is not increasing with time.

6. Conclusions

[61] We find that, to a large extent, the Pacific Plate is a rigid entity. Motion of the plate is well modeled by a single Euler vector (63.75°S, 110.86°E, 0.677°/Myr relative to ITRF2000) with an RMS residual velocity of 0.4 mm/yr.

[62] We find a relative Euler vector between the Pacific and North American plates in close agreement with that of *DeMets and Dixon* [1999]. Our relative Euler vector between the Pacific and Australian plates is much more precisely located than in the NUVEL-1A model of *DeMets et al.* [1994], but it is not significantly different given the uncertainties in the NUVEL-1A model. Our Euler vector is also similar to a recent appraisal of 3-Ma average motion by *Spitzak and DeMets* [1996], with a difference between the models barely significant at the 95% confidence level. We conclude that the PA/AU motion has been essentially steady over at least the past 3 Myr.

[63] Our Pacific-Australian Euler vector predicts a relative plate velocity in the central South Island of New Zealand corresponding to 39–40 mm/yr right-lateral strike slip along the Alpine Fault and 9–10 mm/yr convergence normal to the fault. These values are consistent with results from dense GPS surveys across the South Island and with geological and geochronological evidence on Alpine Fault motion and Southern Alps deformation.

[64] Previous publications have indicated that station CHAT may be moving significantly differently from the majority of the Pacific Plate, and that station FAIR is moving significantly differently from the majority of the

North American Plate. We find, however, that CHAT is moving with the Pacific Plate. Our residual velocity for FAIR is 2.0 mm/yr at 153°, which is close to the 1.5 mm/yr at 168° VLBI estimate of *Ma et al.* [1990] but significantly smaller than the value of 5.0 mm/yr at 125° recently derived by *Kogan et al.* [2000].

[65] Velocities at two sites on the east coast of the South Island of New Zealand indicate that the deformation zone associated with the boundary between the Pacific and Australian plates is larger in extent than has previously been assumed by some authors, with both sites moving ~3 mm/yr relative to the Pacific Plate interior, with a sense of motion opposite to PA/AU relative motion. The permanent GPS tracking site at Dunedin (OUSD) and the campaign site near Christchurch (5508) should not be considered to be moving as part of the rigid Pacific Plate, at least at the present time.

[66] Velocities at the western extremities of the GPS networks in southern California show that these sites exhibit relative motion of 4–5 mm/yr with respect to the Pacific Plate. As in New Zealand, the velocity deficit is approximately parallel to the relative velocity vector between the neighboring plates. While we have attributed some of this relative motion to strain accumulation caused by locked faults, the motion at San Nicolas Island of ~4 mm/yr cannot be explained by simple dislocation models on known faults. We infer that there may be additional active faults to the southwest of San Nicolas Island which accommodate the remaining relative motion.

[67] **Acknowledgments.** We thank all who have assisted in collecting the GPS data, including the operators of the Marcus Island station; the Principal and staff of Xavier High School, Chuuk; Andrew Carman; Vince Belgrave; Jane Forsyth; Don McKnight; Ian Turnbull; Ted Koczynski; David Phillips; Roger Williams; Dion Matheson; the Government of Niue, in particular George Sioneholo; the Government of Samoa, in particular Toelau Iulio; the New Zealand Department of Conservation; the New Zealand Department of Survey and Land Information; Otago University Survey Department for OUSD data; the Australian Survey and Land Information Group for ALIC and KARR data; the Southern California Integrated Geodetic Network for FARB, SCIP, and SNI1 data; and the International GPS Service for IGS data. We thank Dick Walcott, Des Darby, and Chris Scholz, who provided the early impetus for the plate boundary GPS measurements in and near New Zealand. We are grateful to Rupert Sutherland for discussions about the Pacific Plate, Nicola Litchfield for information on faulting offshore of Otago, and Bryan Davy, David Rhoades, Chuck DeMets, and Joann Stock for their constructive comments on the manuscript. The figures were prepared using GMT [*Wessel and Smith*, 1998], Igor (http://www.wavemetrics.com), and Adobe Illustrator. Funding for the measurements and analysis has come from New Zealand Foundation for Research, Science and Technology (FRST) contract CO5811 to GNS, as well as earlier FRST contracts to GNS and Victoria University of Wellington; NASA Dynamics of the Solid Earth grants NAG5-1949 to Lamont-Doherty Earth Observatory (LDEO) and NAG5-1957 to UNAVCO for collection of early New Zealand data; and NSF grants EAR89-15622 and INT92-18010 to LDEO for collection of early data from Chuuk. GNS contribution 1965.

References

Adams, R. D., and R. J. Kean, The Dunedin earthquake, 9 April 1974, part 1, Seismological studies, *Bull. N. Z. Natl. Soc. Earthquake Eng.*, *7*, 115–122, 1974.

Altamimi, Z., P. Sillard, and P. Boucher, ITRF2000: A new release of the International Terrestrial Reference Frame for earth science applications, *J. Geophys. Res.*, *107*(B10), 2214, 10.1029/2001JB000561, 2002.

Argus, D. F., and R. G. Gordon, No-Net-Rotation model of current plate velocities incorporating plate motion model NUVEL-1, *Geophys. Res. Lett.*, *18*, 2039–2042, 1991.

Atwater, T., and J. Stock, Pacific-North America plate tectonics of the Neogene southwestern United States: An update, *Int. Geol. Rev.*, *40*, 375–402, 1998.

Batt, G. E., and J. Braun, The tectonic evolution of the Southern Alps, New Zealand: Insights from fully thermally coupled dynamical modelling, *Geophys. J. Int.*, *136*, 403–420, 1999.

Beavan, J., and J. Haines, Contemporary horizontal velocity and strain rate fields of the Pacific-Australian plate boundary zone through New Zealand, *J. Geophys. Res.*, *106*, 741–770, 2001.

Beavan, J., et al., Crustal deformation during 1994–1998 due to oblique continental collision in the central Southern Alps, New Zealand, and implications for seismic potential of the Alpine Fault, *J. Geophys. Res.*, *104*, 25,233–25,255, 1999.

Bennett, J., W. Rodi, and R. E. Reilinger, Global Positioning System constraints on fault slip rates in southern California and northern Baja, Mexico, *J. Geophys. Res.*, *101*, 21,943–21,960, 1996.

Berryman, K. R., Active faulting and derived PHS directions in the South Island, NZ, *Bull. R. Soc. N. Z.*, *18*, 29–34, 1979.

Bevis, M., et al., Geodetic observations of very rapid convergence and back-arc extension at the Tonga arc, *Nature*, *374*, 249–251, 1995.

Boucher, C., Z. Altamimi, P. Sillard, The ITRF97 International Terrestrial Reference Frame (ITRF97), *Int. Earth Rotation Serv. Tech. Note 27*, Obs. de Paris, Paris, 1999.

Bourne, S. J., T. Arnadottir, J. Beavan, D. Darby, P. C. England, B. Parsons, R. I. Walcott, and P. R. Wood, Crustal deformation of the Marlborough fault zone in the South Island of New Zealand: Geodetic constraints over the interval 1982–1994, *J. Geophys. Res.*, *103*, 30,147–30,165, 1998.

Campbell, H. J., et al., *Cretaceous-Cenozoic Geology and Biostratigraphy of the Chatham Islands, New Zealand, Monograph*, vol. 2, Inst. Geol. Nuclear Sci., Lower Hutt, New Zealand, 269 pp., 1993.

Cande, S. C., and D. V. Kent, Revised geomagnetic polarity timescale, *J. Geophys. Res.*, *100*, 6093–6095, 1995.

Cande, S. C., C. A. Raymond, J. Stock, and W. F. Haxby, Geophysics of the Pitman Fracture Zone and Pacific-Antarctic plate motions during the Cenozoic, *Science*, *270*, 947–953, 1995.

Darby, D. J., and J. Beavan, Evidence from GPS measurements for contemporary plate coupling on the southern Hikurangi subduction thrust and for partitioning of strain in the upper plate, *J. Geophys. Res.*, *106*, 30,881–30,892, 2001.

DeMets, C., and T. H. Dixon, New kinematic models for Pacific-North America motion from 3 Ma to present, I, Evidence for steady motion and biases in the NUVEL-1A model, *Geophys. Res. Lett.*, *26*, 1921–1924, 1999.

DeMets, C., R. G. Gordon, D. F. Argus, and S. Stein, Effect of recent revisions to the geomagnetic reversal time scale on estimates of current plate motions, *Geophys. Res. Lett.*, *21*, 2191–2194, 1994.

Dixon, T. H., A. Mao, and S. Stein, How rigid is the stable interior of the North American plate?, *Geophys. Res. Lett.*, *23*, 3035–3038, 1996.

Dixon, T., F. Farina, C. DeMets, F. Suarez-Vidal, J. Fletcher, B. Marquez-Azua, M. Miller, O. Sanchez, and P. Umhoefer, New Kinematic Models for Pacific-North America Motion from 3 Ma to Present: Evidence for a "Baja California shear zone", *Geophys. Res. Lett.*, *27*, 3961–3964, 2000.

Dong, D., T. A. Herring, and R. W. King, Estimating regional deformation from a combination of space and terrestrial geodetic data, *J. Geod.*, *72*, 200–214, 1998.

Ekstrom, G., and B. Romanowicz, The 23 May 1989 Macquarie Ridge earthquake: A very broad band analysis, *Geophys. Res. Lett.*, *17*, 993–996, 1990.

Feigl, K., et al., Space geodetic measurements of crustal deformation in central and southern California, 1984–1992, *J. Geophys. Res.*, *98*, 21,677–21,712, 1993.

Freymueller, J. T., M. H. Murray, P. Segall, and D. Castillo, Kinematics of the Pacific-North America plate boundary zone, northern California, *J. Geophys. Res.*, *104*, 7419–7441, 1999.

Herring, T. A., GLOBK global Kalman filter VLBI and GPS analysis program, version 4.1, Mass. Inst. of Technol., Cambridge, 1999.

Johnson, H. O., and D. C. Agnew, Correlated noise in geodetic time series, final technical report to USGS, U.S. Geol. Surv., Menlo Park, Calif., 2000.

Johnstone, T., A seismic reflection investigation of the extent and geometry of recent northeast-trending faults on the Otago shelf, M. Sc. thesis, Univ. of Otago, Dunedin, New Zealand, 1990.

Kato, T., et al., Initial results from WING, the continuous GPS network in the western Pacific region, *Geophys. Res. Lett.*, *25*, 369–372, 1998.

King, R. W., and Y. Bock, Documentation for the GAMIT GPS analysis software, release 9.6, Mass. Inst. of Technol., Cambridge, 1999.

Knuepfer, P. L. K., Temporal variations in latest Quaternary slip across the Australian-Pacific plate boundary, northeastern South Island, New Zealand, *Tectonics*, *11*, 449–464, 1992.

Kogan, M. G., et al., Geodetic constraints on the rigidity and relative motion of Eurasia and North America, *Geophys. Res. Lett.*, *27*, 2041–2044, 2000.

Langbein, J., and H. Johnson, Correlated errors in geodetic time series:

Implications for time- dependent deformation, *J. Geophys. Res.*, *102*, 591–604, 1997.
Larson, K. M., J. T. Freymueller, and S. Philipsen, Global plate velocities from the Global Positioning System, *J. Geophys. Res.*, *102*, 9961–9981, 1997.
Levitt, D. A., and D. T. Sandwell, Modal depth anomalies from multibeam bathymetry: Is there a South Pacific superswell?, *Earth Planet. Sci. Lett.*, *139*, 1–16, 1996.
Litchfield, N. J., and R. J. Norris, Holocene motion on the Akatore Fault, south Otago coast, New Zealand, *N. Z. J. Geol. Geophys.*, *43*, 405–424, 2000.
Ma, C., J. M. Sauber, L. J. Bell, T. A. Clark, D. Gordon, W. E. Himwich, and J. W. Ryan, Measurement of horizontal motions in Alaska using very long baseline interferometry, *J. Geophys. Res.*, *95*, 21,991–22,011, 1990.
Ma, C., et al., Goddard Space Flight Center VLBI annual report, Goddard Space Flight Cent., Greenbelt, Md., 1995.
Mao, A., C. G. A. Harrison, and T. H. Dixon, Noise in GPS coordinate time series, *J. Geophys. Res.*, *104*, 2797–2816, 1999.
McClusky, S., et al., Global Positioning System constraints on plate kinematics and dynamics in the eastern Mediterranean and Caucasus, *J. Geophys. Res.*, *105*, 5695–5719, 2000.
McNutt, M. K., and K. M. Fischer, The South Pacific Superswell, in *Seamounts, Islands and Atolls*, *Geophys. Monogr. Ser.*, vol. 43, edited by B. H. Keating, pp. 25–34, AGU, Washington, D. C., 1987.
Pearson, C., P. Denys, and K. Hodgkinson, Geodetic constraints on the kinematics of the Alpine fault in the southern South Island of New Zealand, using results from the Hawea-Haast GPS transect, *Geophys. Res. Lett.*, *27*, 1319–1322, 2000.
Peltier, W. R., Ice-age paleotopography, *Science*, *265*, 195–201, 1994.
Pollitz, F., Gravitational viscoelastic postseismic relaxation on a layered spherical Earth, *J. Geophys. Res.*, *102*, 17,921, 1997.
Satake, K., and H. Kanamori, Fault parameters and tsunami excitation of the May 23, 1989, Macquarie Ridge earthquake, *Geophys. Res. Lett.*, *17*, 997–1000, 1990.
Savage, J. C., and R. O. Burford, Geodetic determination of relative plate motion in central California, *J. Geophys. Res.*, *78*, 832–845, 1973.
Savage, J. C., and M. Lisowski, Viscoelastic coupling model of the San Andreas fault along the Big Bend, southern California, *J. Geophys. Res.*, *103*, 7281–7292, 1998.
Savage, J. C., J. L. Svarc, and W. H. Prescott, Geodetic estimates of fault slip rates in the San Francisco Bay area, *J. Geophys. Res.*, *104*, 4995–5002, 1999.
Spitzak, S., and C. DeMets, Constraints on present-day plate motions south of 30°S from satellite altimetry, *Tectonophysics*, *253*, 167–208, 1996.
Taylor, F. W., et al., Geodetic measurements of convergence at the New Hebrides island arc indicate arc fragmentation caused by an impinging aseismic ridge, *Geology*, *23*, 1011–1014, 1995.
Tregoning, P., Is the Australian Plate deforming? A space geodetic perspective, joint special publication, Geol. Soc. of Aust. and Geol. Soc. of Am., Boulder, Colo., in press, 2002a.
Tregoning, P., Plate kinematics in the Western Pacific derived from geodetic observations, *J. Geophys. Res.*, *107*, XXXX, doi:2001JB000406, 2002b.
Tregoning, P., et al., Estimation of current plate motions in Papua New Guinea from Global Positioning System observations, *J. Geophys. Res.*, *103*, 12,181–12,203, 1998.
Walcott, R. I., Modes of oblique compression: Late Cenozoic tectonics of the South Island of New Zealand, *Rev. Geophys.*, *36*, 1–36, 1998.
Wahr, J., T. van Dam, K. Larson, and O. Francis, Geodetic measurements in Greenland and their implications, *J. Geophys. Res.*, *106*, 16,567–16,582, 2001.
Wdowinski, S., Y. Bock, J. Zhang, P. Fang, and J. Genrich, Southern California Permanent GPS Geodetic Array: Spatial filtering of daily positions for estimating coseismic and postseismic displacements induced by the 1992 Landers earthquake, *J. Geophys. Res.*, *102*, 18,057–18,071, 1997.
Wessel, P., and W. H. F. Smith, Free software helps map and display data, *Eos Trans. AGU*, *79*, 579, 1998.
Zhang, J., Y. Bock, H. Johnson, P. Fang, S. Williams, J. Genrich, S. Wdowinski, and J. Behr, Southern California permanent GPS geodetic array: Error analysis of daily position estimates and site velocities, *J. Geophys. Res.*, *102*, 18,035–18,055, 1997.
Zhang, Q., W. Zhu, and Y. Xiong, Global plate models incorporating the velocity field of ITRF96, *Geophys. Res. Lett.*, *26*, 2813–2816, 1999.

J. Beavan, Institute of Geological and Nuclear Sciences, P.O. Box 30-368, Lower Hutt, New Zealand. (j.beavan@gns.cri.nz)
M. Bevis, SOEST, University of Hawaii, HIGP, 1680 East-West Road (POST 602), Honolulu, HI 96822, USA. (bevis@soest.hawaii.edu)
T. Kato, Earthquake Research Institute, University of Tokyo, No. 1-1, Yayoi 1-chome, Bunkyo-ku, Tokyo 113, Japan. (teru@eri.u-tokyo.ac.jp)
C. Meertens, UNAVCO, P.O. Box 3000, Boulder, CO 80307-3000, USA. (chuckm@unavco.ucar.edu)
P. Tregoning, Research School of Earth Sciences, The Australian National University, Canberra, A.C.T., 0200, Australia. (pault@rses.anu.edu.au)